

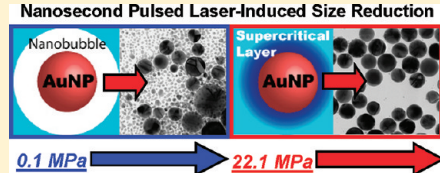
Methodological Improvement in Pulsed Laser-Induced Size Reduction of Aqueous Colloidal Gold Nanoparticles by Applying High Pressure

Daniel Werner, Tomoyuki Ueki, and Shuichi Hashimoto*

Department of Ecosystem Engineering, The University of Tokushima, Tokushima 770-8506, Japan

Supporting Information

ABSTRACT: By applying high pressures well above the critical pressure of water (22.1 MPa), we prepared gold nanoparticles (Au NPs) using a nanosecond pulsed laser-induced size-reduction technique. The Au NPs thus obtained exhibited a narrow size distribution and size-selectivity dependent on the applied laser energy density (fluence). This is significant because previous attempts under ambient pressure failed to achieve such size-selective generation. Spherical Au NPs of diameters 46 and 33 nm, with a standard deviation of only 2–3 nm, were obtained at the expense of original faceted 58 nm Au NPs. We ascribed our results to the formation of a supercritical water layer surrounding the liquid droplet NP transformed by laser heating. The supercritical layer originates from heat transfer from the particle, leading to water temperatures above the critical point of 647 K. The supercritical water layer acts as an effective heat sink for photothermal layer-by-layer size reduction to release small fragments, leaving behind a core particle. The supercritical water can retard evaporation of atoms and clusters from the droplet, thus controlling the evaporation rate. In contrast, at an ambient pressure of 0.1 MPa, the size reduction takes place inside the bubble that can form through the explosive evaporation of superheated water. In this case, particles of various sizes were produced, accompanied by connected structures. This is because thermal insulation is achieved inside the bubble, where the size reduction takes place with insufficient cooling. This study clearly showed nanosecond laser-induced size reduction of Au NPs, better than that achieved previously, by introducing an additional parameter, pressure. This study provides a refined method for size control in laser ablation NP generation. We expect that a rich chemistry can proceed in this transient supercritical water layer surrounding the NP droplets as a reaction medium.



INTRODUCTION

Plasmonic nanoparticles (NPs) such as those of gold and silver have extremely large absorption and scattering cross sections in the visible light regions because of the localized surface plasmon resonance (LSPR) band.¹ The LSPR, a collective electron charge oscillation coupled with light, is responsible for the enhancement of the incident electromagnetic field in the near-field regime.^{2,3} At the same time, excitation of the LSPR band through light absorption contributes to a spontaneous temperature rise in the particle–lattice system, followed by heat dissipation to the surrounding medium.⁴ These properties permit plasmonic NPs to exhibit intriguing time- and space-dependent responses to interaction with pulsed lasers, giving rise to rich physics and chemistry. For instance, laser-induced relocation and release of gold NPs (Au NPs) or nanostructures from a substrate surface have been demonstrated for excitation by both femtosecond and nanosecond lasers.^{5–7} Nanoholes can be prepared on the Au-NP-modified surfaces of glass^{8,9} and polymers^{10,11} by exposure to single-shot nanosecond pulses of intensities far lower than the ablation threshold of the substrates. Moreover, nanobubbles capable of killing tumor cells are formed through explosive evaporation on the particle surfaces where water molecules are superheated ($\sim 300^\circ\text{C}$) as a result of heat transfer from the NP.^{12,13} Interestingly, pulsed laser irradiation of gold nanorods induced transformations to spherical and small particles.^{14,15}

The pulsed laser-induced modification represented by the size reduction of NPs constitutes a core technology in liquid-phase laser-ablation-based NP generation. The technique has attracted a great deal of attention in recent years because of its flexibility and productivity potentials, complementary to chemical synthetic methods.^{16–19} From a mechanistic point of view, two models, namely photothermal melting–evaporation and the Coulomb explosion hypotheses, have been proposed. The former postulates effective absorption of laser energy to change the shape of an NP by surface melting and eventual size reduction because of evaporation from both the particle surface and the entire particle.^{20–24} In contrast, the Coulomb explosion mechanism presumes ejection of large numbers of electrons to generate multiply ionized NPs, which undergo spontaneous fission because of charge repulsion.^{25–30} Recent investigations have revealed that the size reduction mechanism strongly depends on the excitation pulse duration. For femtosecond laser excitation, the mechanism is explained by the Coulomb explosion, whereas, in marked contrast, nanosecond pulsed laser excitation of Au NPs results in photothermal evaporation events.^{31,32}

Received: December 15, 2011

Revised: February 14, 2012

Published: February 29, 2012

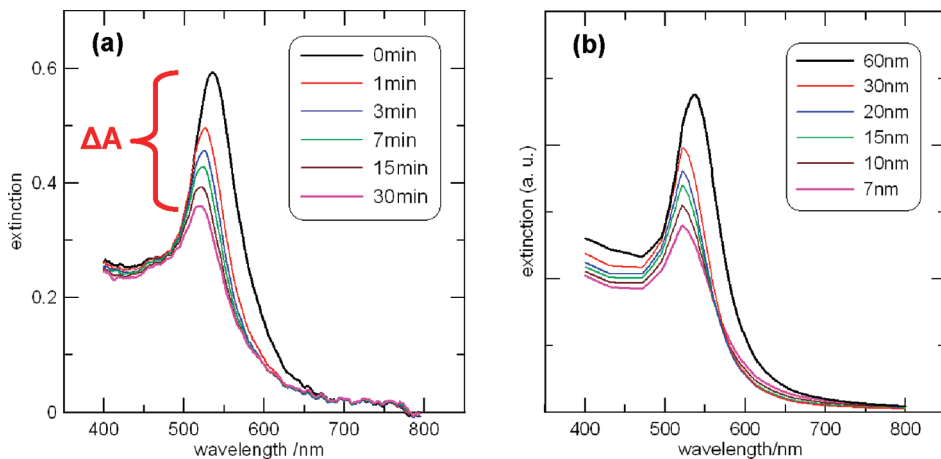


Figure 1. (a) *In situ* spectra of original Au NPs of diameter 58 nm in aqueous solution obtained during pulsed laser irradiation at 532 nm with an energy density of 56.6 mJ cm⁻² under an external pressure of 60 MPa. The symbol ΔA represents the reduction in the peak intensity of the LSPR band on irradiation for 30 min (18 000 shots, 10 Hz). (b) A series of simulated extinction spectra based on the Mie theory for the size reduction of initial 60 nm Au NPs dispersed in water ($n = 1.33$). Note here that the total atomic concentration of Au was kept constant, and thus this spectral change includes the increase in the number of particles accompanying the size reduction. The calculation reproduces the depression in the LSPR band.

Although much effort has been devoted to promoting a deeper understanding of the mechanistic aspects, morphological control in laser-induced size reduction still needs further improvements. In particular, bubble formation during laser irradiation at ambient atmospheric pressure for a water layer directly surrounding NPs can be a major obstacle to the controlled NP cooling that is anticipated in the liquid environment. Transmission electron microscopy (TEM) observations of laser-induced fragments have revealed that nanosecond laser irradiation generated coalesced particle aggregates or necklace-like network structures.^{20,24,33} We therefore decided to improve the particle size selectivity and size distribution by applying a high pressure to the solution, on the following two grounds:

(1) Suppression of laser-induced bubbles during the size reduction may allow fast cooling of NPs by enhancing heat transfer to the surrounding medium. In this regard, it is instructive to refer to a recent work on laser ablation in pressurized water. Sasaki and co-workers demonstrated that the application of an external pressure below 30 MPa to ambient water can reduce the size of cavitation bubbles as well as giving control over the dynamics of such bubbles in the nanosecond laser ablation of a Ti target.^{34,35}

(2) With increasing external pressure, slower evaporation of Au NPs is anticipated as a result of boiling point elevation. This could be another factor for controlling particle size, a point that has not been addressed previously.

Thus, we planned a nanosecond laser size reduction study of Au NPs at various pressures that far exceed the critical pressure of water, 22.1 MPa.

Here we show that external pressure has a significant effect that has not been reported previously. The size reduction mechanism was basically photothermal in nature: the gradual size reduction was observed to depend on both the laser energy density (mJ cm⁻²) and the irradiation period. The threshold laser energy (fluence) for size reduction increased significantly with increasing pressure on excitation of gold particles of diameter 58 ± 5 nm using a nanosecond pulsed laser at 532 nm. The threshold laser energy at 150 MPa was more than twice the value at atmospheric pressure of 0.1 MPa. Notably, we observed better controllability of particle size at high pressures. Narrow size

distributions with size selectivity have not been achieved in previous laser ablation or size reduction experiments under ambient conditions.^{16,17,20–30} The present study revealed that pressurizing the liquid is a promising way of controlling particle size and size distribution.

EXPERIMENTAL SECTION

Au NPs were obtained from British Biocell International (EMGC60: 58 ± 5 nm diameter, Supporting Information Figure S1; EMGC100: 100 ± 7 nm diameter, Supporting Information Figure S2). Laser irradiation of 0.4 mL aliquots of aqueous colloidal Au NP solutions contained in a quartz cuvette (optical path length 4.0 mm, width 4.0 mm, length 25 mm) was conducted using the second and third harmonics of a Nd:YAG laser (Continuum, Surelite I-10). The particle concentration of 58 nm NPs was 2.6×10^{10} mL⁻¹, and that of 100 nm NPs was 5.6×10^9 mL⁻¹. The NP solutions were not agitated during the irradiation. The laser parameters were as follows: wavelength, 532 and 355 nm; repetition rate, 10 Hz; pulse width, 5–6 ns full width at half-maximum; beam diameter, 4.2 ± 0.2 mm for 532 nm and 4.5 ± 0.2 mm for 355 nm. The cuvette was placed in a hydrostatically pressurized container (≤ 400 MPa) similar to the one described previously in the literature.³⁶ A 150 W short-arc Xe lamp (Hamamatsu, L2274) was used as a monitor light for the *in situ* spectroscopic measurements, in which the light extinction (absorption and scattering) signals were detected by a UV-vis multichannel spectrophotometer (StellaNet, BlueWave). The light was collected by an optical fiber and fed to the multichannel spectrophotometer. The laser beam was blocked by a shutter during the spectral measurements. TEMs of the particles were recorded on a JEM-2100F (JEOL) microscope operated at 200 kV. Specimens for the TEM measurements were prepared by placing one drop of a sample solution onto a support made of Cu mesh coated with an evaporated 13 nm thick carbon film. The support was dried in air on a hot plate at 40–60 °C. This process was repeated twice to increase the NP concentration on the TEM grid. The preparation of TEM specimens was carried out on the same day as the laser irradiation. Software, Image J, was used for processing particle images.

■ RESULTS AND DISCUSSION

1. Laser-Fluence-Dependent and Pulse-Number-Dependent Size Reduction at High Pressures. Extinction spectra represented by the LSPR band exhibit size-dependent resonance peaks at wavelengths from 520 to 590 nm for Au NPs of diameter 10–100 nm in water (refractive index $n = 1.33$). Figure 1a shows an example of extinction spectral changes of aqueous 58 ± 5 nm Au NPs on excitation of the LSPR band by a 532 nm pulsed laser for different time periods.

A blue shift and remarkable intensity reduction in the LSPR band peak suggest size reduction of the Au NPs.¹ This was confirmed by the TEM images shown below (Figures 3 and 5). For reference, a simulated spectral change for the size reduction of a gold sphere of diameter 60 nm, based on the Mie theory, is given in Figure 1b.³⁷ Figure 1b reproduces satisfactorily the experimentally observed *in situ* spectra. We use ΔA , the change in the LSPR band peak intensity resulting from 30 min of irradiation at 10 Hz (18 000 shots), as a measure of size reduction dependence on energy density (mJ cm^{-2}). Figure 2 shows ΔA at 18 000 shots as a function of laser energy density for 58 nm Au NPs at various pressures.

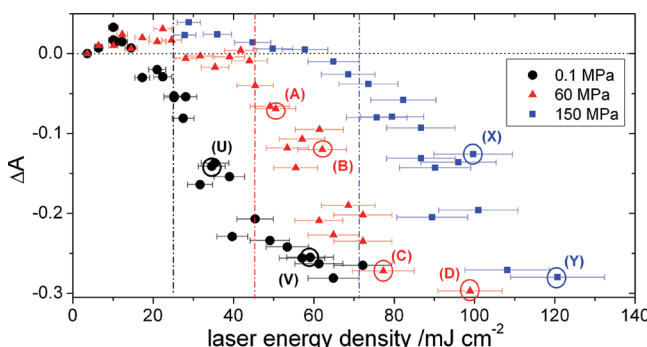


Figure 2. Plots of experimental ΔA , the change in the LSPR band peak intensity, after 18 000 shots (30 min, 10 Hz, 532 nm) vs laser energy density for 58 nm Au NPs dispersed in aqueous solution at three different external pressures: 0.1 MPa (black circles), 60 MPa (red triangles), and 150 MPa (blue squares). The vertical dashed-dotted lines indicate the experimentally estimated size-reduction thresholds. The circled data points correspond to laser intensities at which TEM images were acquired. The TEM images are given in Figure 3 as well as Figures S5 and S6.

The effect of external pressure is remarkable. An increase in the laser energy density results in a distinct reduction in the ΔA signal, indicative of size reduction of the original Au NPs. With increasing pressure, a slower decrease in ΔA was recorded for a given laser intensity. This causes a pressure-dependent shift of the ΔA vs laser energy density curves to the high-energy side, suggesting a greater difficulty in size reduction. Prior to the size reduction, a slight increase of ~ 0.04 was noted for ΔA at peak values from the initial extinction of 0.60 ± 0.03 . This could be the result of increased volumes of monocrystalline lattice structures within a particle as a result of pulsed laser-induced annealing. The Au NPs were prepared by a citrate reduction method that may generate a multicrystalline structure containing crystal defects such as grain boundaries. The defects give increased damping of the conduction electrons, causing a decreased extinction.¹

Figure 3 shows the laser energy density-dependent TEM photographs and corresponding size distributions after 18 000 laser shots at 60 MPa. The laser-treated Au NPs typically show

very spherical shapes, as a result of surface melting or entire melting processes.^{20,21,24,32}

Here, NPs of diameter smaller than 9 nm were not counted because of their very large number. Instead, we focused our attention on the fate of the original particles rather than the small particles ejected from the original Au NPs. The TEM images show that with increasing laser intensity the resulting size distributions exhibited a gradual size reduction of the original 58 nm Au NPs. This result is in accord with the photo-thermal size reduction mechanism, in which layer-by-layer evaporation from the particle surface leads to a bimodal size distribution.^{21,22,24} Bimodal means that one group consists of the remaining cores of the original Au NPs (core particles), and the other consists of the fragments (small fragments) released from the outermost surface. Notably, the minimum average core diameter was not reduced to below 30 nm for a laser power up to 100 mJ cm^{-2} . Only at a high intensity— 132 mJ cm^{-2} —was a slight shift to smaller core NPs, of 28 nm on average, with a noticeable contribution (9%) from below 9 nm particles, obtained. In contrast, at 0.1 MPa (1 atm), the original Au NPs were reduced to 10 nm without great difficulty, and a broad size distribution resulted (Supporting Information Figure S3). The average sizes were 6–8 nm, and some snake-like connected structures were observed. However, the laser-induced fragments obtained at 60 MPa, with an average diameter of 3–5 nm, were much smaller and well separated from each other.

The significant effect of external static pressure on the remarkable size-selective formation of Au NPs is shown in Figure 4. Here the size distributions obtained at 60 MPa after 54 000 shots (3 times greater than the number of shots in Figure 3) is given. Laser energy densities similar to those used for points B and C in Figure 2 were used. At a laser power of 61.4 mJ cm^{-2} , an average diameter of 46 nm with a narrow size distribution of only ± 3 nm was calculated from the standard deviation of the Gaussian fit (Figure 4a). By increasing the laser intensity to 83.7 mJ cm^{-2} , Au NPs with an average diameter of 33 nm with a size distribution of ± 2 nm were obtained at the expense of the original NPs of diameter 58 nm (Figure 4b). Additionally, the size distributions of Au NPs at 150 MPa after 18 000 shots were measured at two laser intensities. The results are basically the same as those obtained at 60 MPa (see Supporting Information Figure S4).

By the application of high external pressures, greatly improved size distributions, which also depend on laser energy densities, were obtained with a minimum average size of 30 nm. The observed 30 nm Au NPs are extremely resistant to further size reduction; extremely high laser powers have to be applied to split the NPs further. This means that we can selectively isolate these particles by ultracentrifugation, for instance. Importantly, these observations could not be made at 0.1 MPa (1 atm) (Figure S3). In short, at 0.1 MPa, a highly controllable size distribution is not feasibly attained by applying nanosecond pulsed lasers.

2. Size Reduction as a Function of External Pressure. In order to reveal more precisely the effects of external pressure on the mean size and size distribution of Au NPs, TEM images at various pressures were acquired after exposure to laser pulses (532 nm) for 30 min (18 000 shots) (Figure 5).

At a pressure of 10 MPa, a broad size distribution reminiscent of that at 0.1 MPa was obtained. The particle sizes ranged from 9 to 58 nm in diameter, with the most abundant population being between 9 and 11 nm (Figure 5A). The TEM observations at 15 and 25 MPa (Figure 5B) were not much

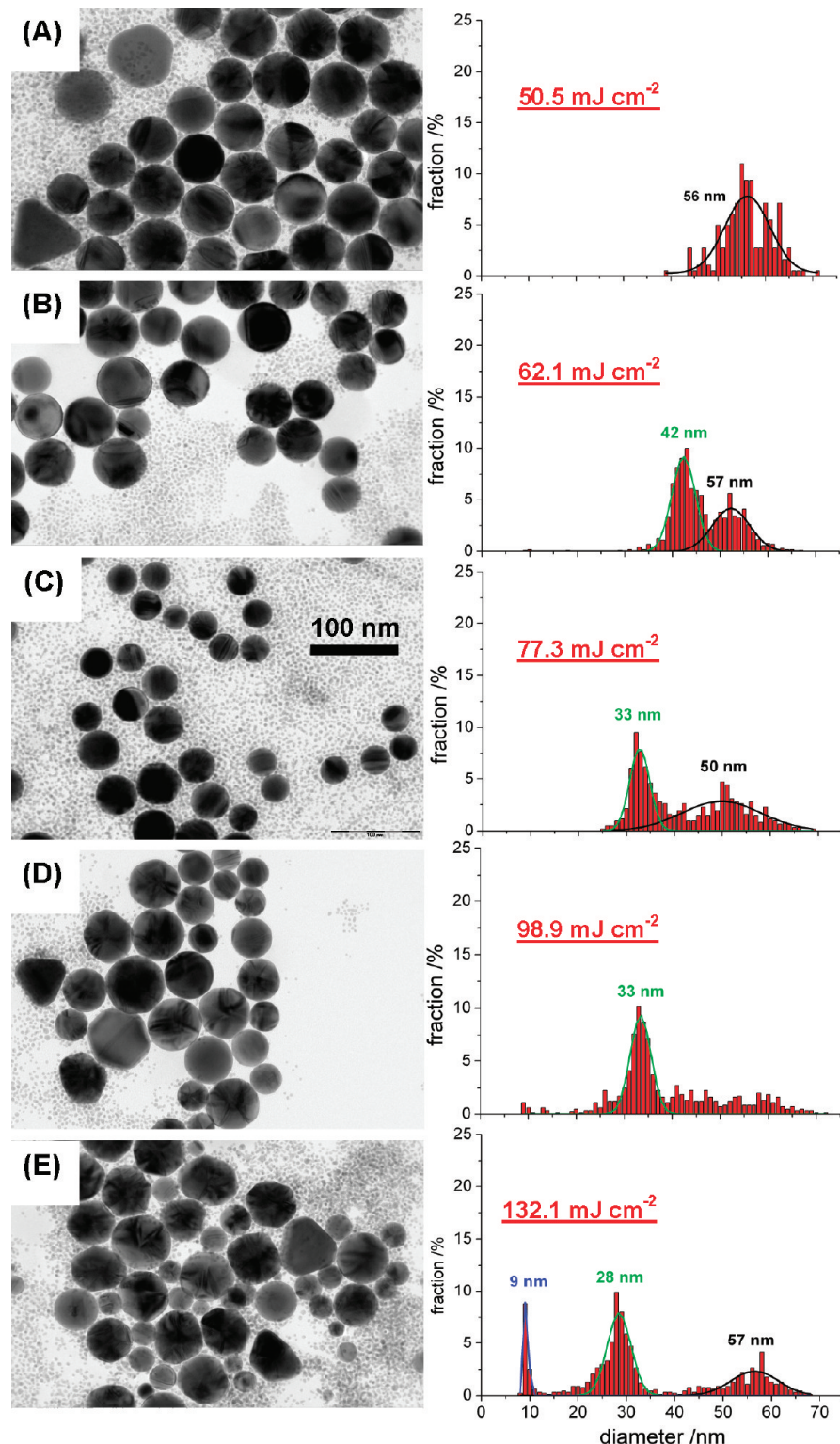


Figure 3. Particle images (TEM photographs) and corresponding size distributions at 60 MPa obtained at different laser energy densities after 18 000 shots (30 min, 10 Hz, 532 nm) for original 58 nm Au NPs. Particle numbers of 500 to 1000 NPs were measured. NPs with diameters smaller than 9 nm were not measured. The 100 nm scale bar is applicable to all TEM images.

different from those at 10 MPa. At pressures \leq 25 MPa, a fraction with sizes of 9–11 nm dominated, and the minimum core diameter remained \sim 10 nm, regardless of the pressure. However, at pressures \geq 30 MPa, the minimum core diameter suddenly increased to 32–35 nm. The minimum core sizes are shown in Figure 6 as a function of external pressure.

The onset of the sudden transition observed corresponds approximately to the occurrence of supercritical water.³⁸ When the water layer surrounding the Au NPs is heated to temperatures above the critical temperature (647 K), resulting from heat transfer from the particle, the supercritical state is formed at pressures \geq 22.1 MPa. Our results strongly suggest

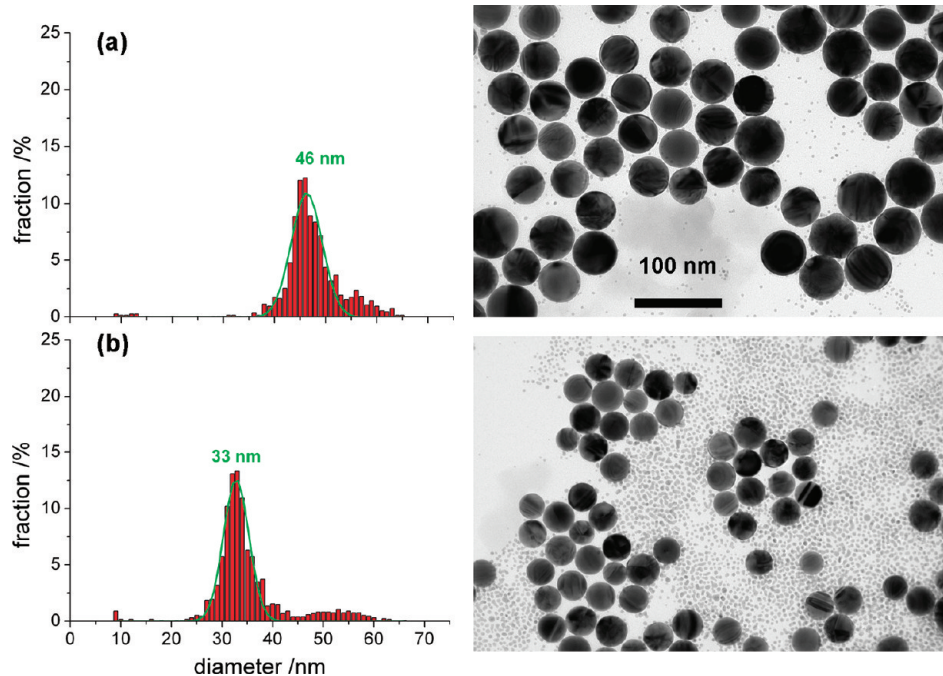


Figure 4. Size distributions and TEM micrographs of Au NPs of average diameter 58 nm at 60 MPa after 54 000 pulses (90 min, 10 Hz, 532 nm). The laser intensities used were similar to those used at points B and C in Figure 2: (a) 61.4 mJ cm^{-2} and (b) 83.7 mJ cm^{-2} . The numbers of particles measured were 1029 in (a) and 1345 in (b).

the occurrence of a supercritical state at pressures >25 MPa because the laser excitation of NPs by the nanosecond laser can raise the water temperature above the critical temperature (see below). Thus, the laser-induced supercritical state is responsible for the observation of a minimum core diameter of 30–35 nm, without undergoing further size reduction. Note that the laser power has to be increased at higher external pressures to observe a similar extent of reduction in ΔA signals (Figure 2). The Au NPs of diameter ~ 30 nm exhibited resistance to further size reduction; i.e., surface evaporation seems to be increasingly difficult once the critical pressure is reached.

Another notable pressure-dependent observation is the morphology of the fragments. Figure 7 compares the TEM photographs of the small particles released at 0.1 and 60 MPa, together with *in situ* spectra. Inspection of Figure 7 reveals that relatively long connected structures are formed as a result of laser irradiation at 0.1 MPa (Figure 7a and Figure S3). The average dimension of these structures is approximately 6–8 nm in width at 0.1 MPa and 3–4 nm at pressures above 30 MPa. At 60 MPa, well above the critical pressure of water, ejected Au NPs were well separated, and the connected structures were totally absent (Figure 7b, also Figures 3 and 5). Thus, appreciably small and homogeneously sized Au NPs were obtained; this can also be related to the occurrence of supercritical water. The TEM observations were supported by the extinction spectral changes given in Figure 7. A significant increase in the near-IR region,³⁹ associated with coagulation and coalescences, with increasing irradiation time was only observed at 0.1 MPa.

The effects of excitation wavelength and initial particle size on size reduction were examined. Since no significant effect of excitation wavelength was observed, the result was placed in Supporting Information Figure S5. Figure 8 shows the results of size reduction of 100 ± 7 nm Au NPs on irradiation with

54 000 shots (90 min, 10 Hz at 532 nm) at two different laser energy densities under a pressure of 60 MPa.

As observed for 58 nm Au NPs, we again met great difficulty in size reduction to very small particles, as opposed to the observation at 0.1 MPa. The size reduction of the core particles stopped for spherical Au NPs with average diameters of 37 ± 4 nm, generated from the original 100 nm particles, irradiated at 75.8 mJ cm^{-2} (Figure 8b). Consistent with the layer-by-layer mechanism, a greater number of pulses were necessary to induce size reduction of the original 100 nm particles to an extent similar to that of 58 nm Au NPs (a minimum size of ~ 33 nm). Supporting Information Figure S6 compares the size distributions at 60 and 0.1 MPa after 18 000 shots (30 min, 10 Hz at 532 nm). The result at 0.1 MPa shows that no size-selective generation is possible. Small particles under 15 nm in diameter dominated.

3. Explanation for Pressure-Dependent Evaporation Thresholds.

The boiling point of bulk gold depends critically on the external pressure. According to the Clausius–Clapeyron equation, boiling points increase in a nonlinear manner as the pressure increases.⁴⁰ Supporting Information Figure S8 gives the calculated boiling points (T_{bp}) of bulk gold as a function of external pressure from 0.1 to 400 MPa. For instance, T_{bp} is calculated to be 4800 K (10 MPa), 5600 K (30 MPa), 6200 K (60 MPa), and 7700 K (200 MPa). The critical point of gold has been determined experimentally to be $T_{\text{cp}} = 7400$ K with $p_{\text{cp}} = 530$ MPa.⁴¹ The distinct shifts observed for the laser energy density– ΔA curve to the higher energy side (Figure 2) can primarily be explained by an increased T_{bp} at high pressures. The increased T_{bp} causes greater difficulty in photothermal evaporation: a higher laser energy density is necessary to facilitate the surface evaporation of Au NPs as the pressure increases.⁴² In contrast, the melting point of bulk gold within the range of applied pressures here stays practically constant because of its weak pressure dependence. Previous studies have

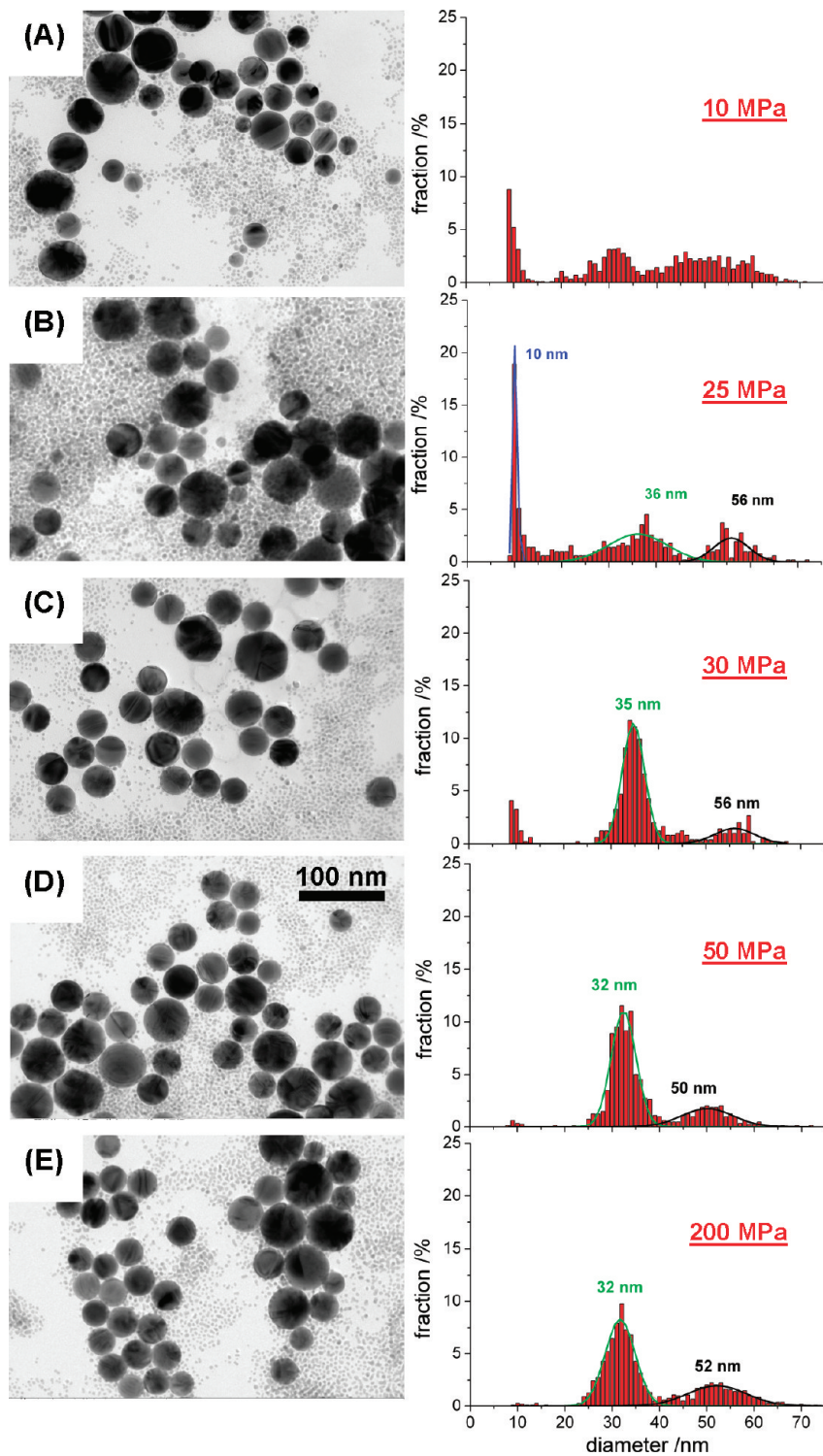


Figure 5. Particle images (TEM photographs) and corresponding size distributions obtained at different pressures for original 58 nm Au NPs after 18 000 laser pulses (30 min, 10 Hz, 532 nm). The laser intensities were increased with increasing external pressures to obtain similar values of ΔA of between -0.252 and -0.291 for all samples. The laser energy densities applied are (A) 59.2, (B) 65, (C) 72.2, (D) 80.8, and (E) 129.9 mJ cm^{-2} . Between 500 and 1300 NPs were measured, and particles with diameters smaller than 9 nm were ignored. The 100 nm scale bar is applicable to all TEM images.

shown that pressures of the order of gigapascals are necessary to increase the melting point by a few hundred kelvin.^{43–45} This means that the melting temperature of bulk gold at 400 MPa is only 30 K higher than that at 0.1 MPa (1 atm).⁴⁵

4. Suppressing Effects of High Pressure on Nanobubble Formation from Surrounding Water.

As briefly mentioned, nanosecond pulsed laser excitation of aqueous Au NPs allows the particle temperature to rise to the boiling point, causing evaporation, depending on the laser energy.³¹ At the same time, the temperature of the surrounding water also increases as a result of heat transfer at the NP surface, followed by heat diffusion within the water. The simulated temperature

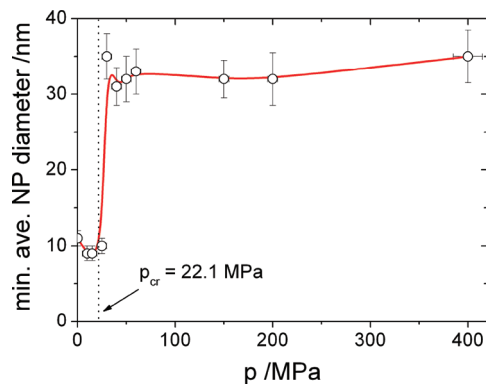


Figure 6. Experimentally obtained minimum average Au NP diameter as a function of external pressure. The vertical error bars indicate the standard deviation of the Gaussian fit of the histograms (see Figure 4). The uncertainties in the pressure gauges are ± 15 MPa for pressures above 200 MPa and ± 5 MPa for pressures below 200 MPa. The vertical dashed line shows the critical pressure of water, 22.1 MPa.

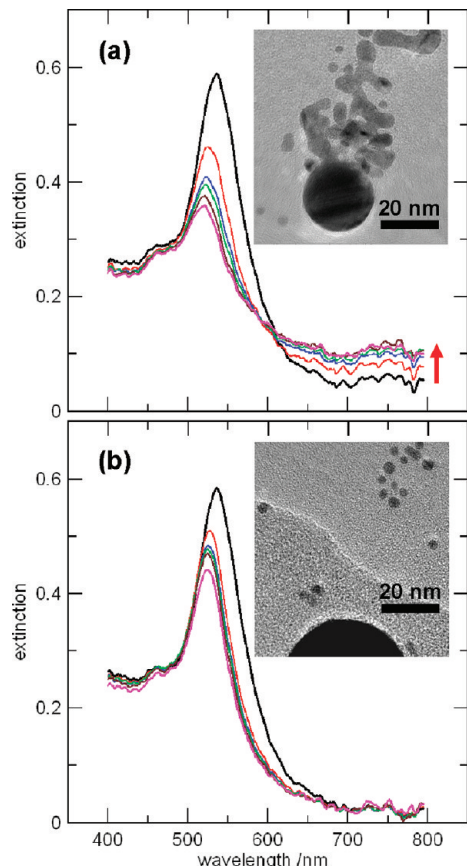


Figure 7. *In situ* spectra together with TEM photographs for original 58 nm diameter Au NPs, taken after 18 000 shots at (a) 39.7 mJ cm^{-2} (0.1 MPa) and (b) 55.5 mJ cm^{-2} (60 MPa). The excitation laser wavelength was 532 nm. The red arrow in (a) indicates the extinction increase in the near-IR region with increasing irradiation period. The spectra were measured after 0, 1, 3, 7, 15, and 30 min.

distribution of a 60 nm Au NP submerged in water on excitation by a 532 nm nanosecond pulse of 5 mJ cm^{-2} is given in Figure 9 for three time delays. Details of the simulation procedure have been described in the literature.³¹

Under these conditions, a quasi-thermal equilibrium is established between the NP-lattice temperature, T_L , and the water

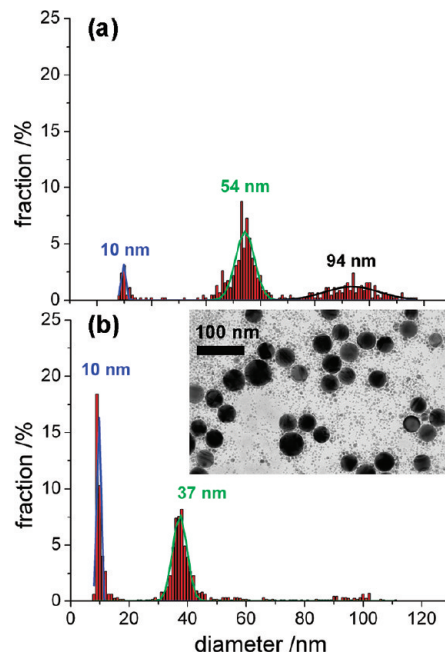


Figure 8. Size distribution of initial 100 nm diameter aqueous colloidal Au NPs after 54 000 pulses (90 min, 10 Hz, 532 nm). The laser energy densities were (a) 50.5 and (b) 75.8 mJ cm^{-2} . The inset in (b) shows a corresponding TEM image. The numbers of particles measured were (a) 456 and (b) 1097. The corresponding *in situ* spectra are given in Supporting Information, Figure S7.

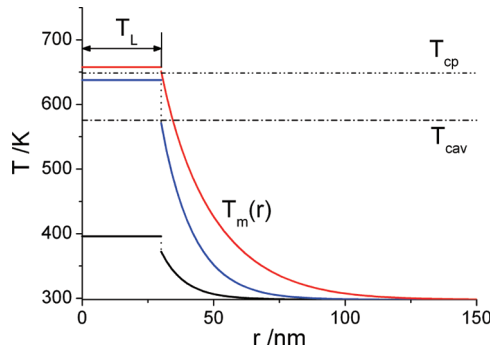


Figure 9. Calculated temperature profile of water surrounding a 60 nm diameter Au NP excited by a laser power density of 5 mJ cm^{-2} at 532 nm (pulse duration: $\tau_p = 5 \text{ ns}$) as a function of the radial distance, r , from the NP center. The time delays are 7.5 ns (black curve), 10 ns (blue curve), and 15 ns (red curve). The starting point of the simulation was $-2\tau_p$ from the maximum position of the Gaussian time profile of a laser pulse. The lattice temperature T_L of the NP is assumed to be uniform because of a large value of thermal conductivity ($318 \text{ W m}^{-1} \text{ K}^{-1}$). Temperatures T_{cp} and T_{cav} represent those of water at the critical point (647 K) and the bubble formation threshold (573 K), which considers the spinodal effect of water.

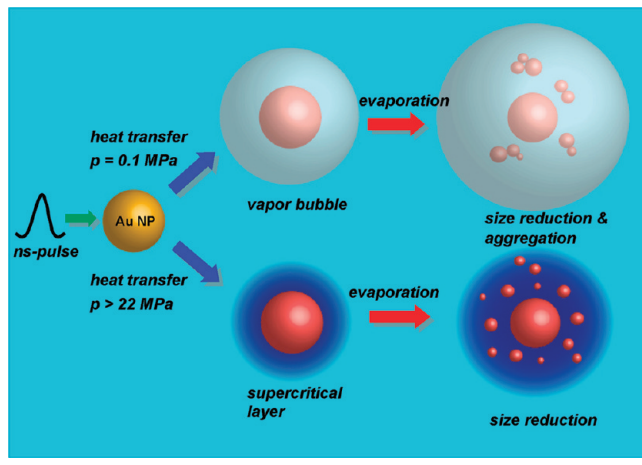
temperature, T_m , at the NP–water interface. The water temperature decreases quickly within a distance of a few tens to hundreds of nanometers from the NP surface. At ambient pressure, a layer of the surrounding superheated water is vaporized as a result of explosive evaporation when the surrounding temperature exceeds a spinodal temperature of ~ 573 K ($\sim 300^\circ\text{C}$).⁴⁶ A bubble thus formed expands into the medium. Unless the external pressure reaches the critical value of 22.1 MPa, the temperature rise causes explosive bubble generation until the water temperature reaches the critical value of

647 K. At this temperature, bubble formation is no longer possible because of the formation of supercritical water. Note that the vapor pressure of ambient water surrounding the NPs as a result of fast evaporation do not exceed 22.1 MPa over the whole heating and cooling process because of the vapor bubble formation. This has been intensively studied for Au NPs exposed to pulsed lasers as well as for nanosecond-pulsed-laser ablation of metal targets.^{34,35,47–49} High vapor pressure can only exist at the initiation of the bubble formation and decreases rapidly during bubble expansion until the bubble collapse.⁵⁰ Thus, a legitimate supercritical water layer can exclusively be established by applying a static external pressure above 22.1 MPa.

Previously, Sasaki and co-workers observed pressure-dependent bubble dynamics in the laser ablation of a Ti target submerged in water.^{34,35} By applying a shadowgraph imaging technique, they observed faster collapse and less vapor bubble generation with increasing external pressure. Our results suggest that the NP fragments are sufficiently small and well separated at external pressures >25 MPa. This strongly suggests that bubble formation could lead to lower stability of fragments during the size-reduction process, causing the fragments to form aggregates because of the insulating effect on heat transfer. This could explain the formation of connected NPs under atmospheric pressure shown in Figure 7 and Figure S3.

Scheme 1 summarizes the laser-induced size reduction of aqueous Au NPs, depending on the external pressure.

Scheme 1. Schematic Illustration of Nanosecond Laser-Induced Size Reduction of Au NPs in Water at Atmospheric Pressure and above the Critical Pressure of 22.1 MPa



The size reduction is assumed to take place by the evaporation of atoms and clusters from Au NP droplets heated above the melting point or even above the boiling point. At pressures below 22.1 MPa, water vapor bubbles surrounding the droplet are formed during the size reduction, causing thermal insulation of the fragments. On the other hand, at pressures above 22.1 MPa, the release of fragments takes place into the supercritical water surrounding the Au NP droplet. The evaporation of gold is supposed to be very slow at high pressures above 22.1 MPa because of inefficient size reduction, as observed above. Consequently, the two different environments realized by the external pressure can seriously affect the fate of both core particles and fragments.

5. Factors Controlling Au NP Size Reduction. We address two points regarding the factors that affect size reduction at

high pressures. The important issue is how we can explain the size selectivity depending on external pressure and laser energy density, represented by Figure 4. We first discuss the influence of the thermal properties of Au NPs submerged in water, followed by examination of our data on the basis of the size-dependent light absorption of Au NPs.

Let us start with the cause of the extremely inefficient size reduction in a solution when a static external pressure well above the critical pressure was applied. Apparently, the low evaporation rates of Au NP droplets in pressurized water is responsible because increased boiling temperatures in supercritical water can make evaporation increasingly difficult. Additionally, the higher thermal conductivity and density of supercritical water than those of water vapor at ambient pressure can contribute to the slow evaporation because of efficient cooling. For instance, the thermal conductivity and density of a steam at atmospheric pressure is $0.021 \text{ W K}^{-1} \text{ m}^{-1}$ and 0.6 kg m^{-3} when evaporation is suppressed, whereas the thermal conductivity and density of water at the critical point are $0.442 \text{ W K}^{-1} \text{ m}^{-1}$ and 3.2 kg m^{-3} , respectively.^{38,42} Furthermore, the heat transfer at the NP–water interface should be considered. The heat transfer at the interface is defined by a heat transfer coefficient F ^{31,51–53}

$$F = \frac{hA_p}{V_p}(T_L - T_m) \quad (1)$$

where the quotient A_p/V_p represents the surface-to-volume ratio of an Au NP; this is larger for smaller NPs. Assuming a constant temperature gradient ($T_L - T_m$) and interfacial thermal conductance h , the heat transfer coefficient F increases with decreasing particle size. In other words, smaller NPs cool faster than bigger NPs,⁵⁴ resulting in increased heat losses for smaller particles. This reduces the NP temperature, and higher laser power has to be applied to promote efficient size reduction. In contrast, heat loss dependent on Au NP size can vanish when nanobubbles are formed because of thermal insulation.^{12,31} Heat losses are therefore negligibly small at external pressures below 22.1 MPa because of bubble generation. Consequently, the combination of lower evaporation rates, greater heat losses, and heat diffusion under high pressures should play an important role in the observed size-selective particle generation.

Second, the assumption that NP size-dependent absorption per particle volume is responsible for the pressure effect was examined. The absorbed laser energy contributing to the temperature rise in an Au NP is defined by³¹

$$S(t) = \frac{C_{\text{abs}}P}{V_p} \quad (2)$$

where P represents the time-dependent intensity profile of the laser pulse. The quantities C_{abs} (absorption cross section) and V_p (particle volume) are obviously size-dependent. The quotient C_{abs}/V_p gives the absorption cross section per NP volume. Figure 10 shows graphically the refractive-index-independent behavior of C_{abs}/V_p in water and vapor.

In water at room temperature ($n = 1.33$), a 50 nm diameter Au NP has the highest C_{abs}/V_p at the excitation wavelength of 532 nm. Particles with diameters smaller or larger than 50 nm have lower values of C_{abs}/V_p , and thus higher laser energy densities are required for heating the NPs to the boiling point of bulk gold. In contrast, Au NPs surrounded by vapor ($n = 1$) show a very weak size-dependent C_{abs}/V_p . The size reduction is therefore expected to proceed regardless of size, but less

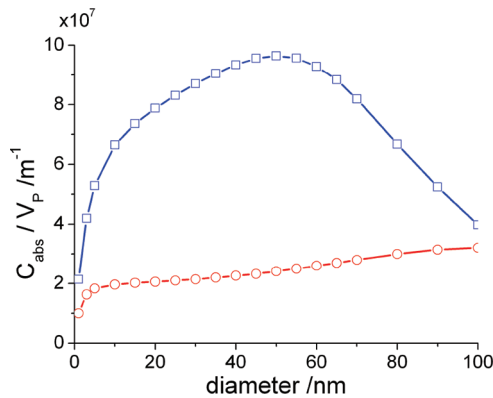


Figure 10. Calculated absorption cross section per volume C_{abs}/V_p dependent on Au NP diameter submerged in water at room temperature, $n = 1.33$ (blue squares), and in vapor, $n = 1$ (red circles). The excitation wavelength was 532 nm. Decreased refractive indices of the surrounding water gave a weaker Au NP size dependence of the absorption efficiencies.

efficiently. In the case of actual excitation, the absorption of laser light by Au NPs starts at ambient temperature ($n = 1.33$), but the temperatures of the NP and the surrounding water rise independently during the pulse duration of 5 ns. Phase transitions of the NP and water also take place during the pulse. These dynamic events hamper quantitative analysis. The experimental laser-induced size reduction of the Au NPs of diameter 100 nm (Figure 8) showed results similar to those for 60 nm Au NPs (Figure 2). This suggests that the size-dependent absorption per particle volume cannot be a critical factor in controlling the size selectivity observed at high pressures. This is because a lower value of C_{abs}/V_p can be predicted for 100 nm Au NPs than for 30 nm particles (Figure 10, $n = 1.33$).

A quantitative discussion is not possible at present because of difficulties in simulating the time- and laser-energy-dependent temperatures of Au NP in supercritical water.

CONCLUSION

The nanosecond laser-induced size reduction of aqueous colloidal Au NPs under high pressures above the critical pressure of water (22.1 MPa) provided previously unreported useful information. Importantly, a supercritical water layer can be generated around a liquid droplet NP that is formed melting as a result of direct laser heating. This NP droplet simultaneously heats up the surrounding water to temperatures above the critical temperature. Although the supercritical water can be formed transiently, this can seriously affect the size reduction of the droplets. Size reduction as a result of photothermal evaporation is significantly retarded under high pressures, primarily because of the boiling point elevation. Most strikingly, layer-by-layer size reduction stops at a certain size, depending on the laser energy density, under external pressures >25 MPa. For instance, particles with average diameters of 46 and 33 nm were prepared with a remarkably narrow size distribution of $\pm(2-4)$ nm at the expense of 58 nm aqueous Au NPs. The minimum core diameter of ~ 30 nm was achieved; further size reduction was not feasible at laser energy densities between 80 and 130 mJ cm⁻² at 60 MPa. The absence of vapor bubbles, which is typical of water under pressures below 22.1 MPa, is an important factor for this observation because bubbles enforce thermal insulation of the NP droplet. In contrast, supercritical water is capable of cooling the NP droplet much more

effectively. Supercritical water may slow down the evaporation of the NP droplet more than vapor bubbles do. This is because an extremely high vapor pressure is necessary to overcome the external pressure. These factors are assumed to play a key role in the better control of the size reduction of Au NPs in pressurized water than in ambient water. These results could provide useful methods for size-selective production of Au NPs, which has not been achieved within the framework of laser ablation generation of NPs in liquids. This could revitalize the conventional ligand-free and swift technique of liquid-phase laser NP generation by taking advantage of pressure.

ASSOCIATED CONTENT

S Supporting Information

Supplementary particle images (TEM micrographs) and corresponding size distributions of Au NPs, pressure-dependent boiling point of bulk gold, and pressure-dependent optical properties of Au NPs and water. This material is available free of charge via the Internet at <http://pubs.acs.org>.

AUTHOR INFORMATION

Corresponding Author

*E-mail: hashi@eco.tokushima-u.ac.jp.

Notes

The authors declare no competing financial interest.

ACKNOWLEDGMENTS

Financial support from KAKENHI (no. 23310065) and The Amada Foundation (AF-2011201) is gratefully acknowledged. A JSPS fellowship to DW (no. 201107976) is also gratefully acknowledged.

REFERENCES

- (1) Kreibig, U.; Vollmer, M. *Optical Properties of Metal Clusters*; Springer: Berlin, 1995.
- (2) Gray, S. K. *Plasmonics* **2007**, *2*, 143–146.
- (3) Bharadwaj, P.; Deutsch, B.; Novotny, L. *Adv. Opt. Photonics* **2009**, *1*, 438–483.
- (4) Hartland, G. V. *Chem. Rev.* **2011**, *111*, 3858–3887.
- (5) Habenicht, A.; Olapinski, M.; Burmeister, F.; Leiderer, P.; Boneberg, J. *Science* **2005**, *309*, 2043–2045.
- (6) Huang, W.; Qian, W.; El-Sayed, M. A. *J. Am. Chem. Soc.* **2006**, *128*, 13330–13331.
- (7) Tabor, C.; Qian, W.; El-Sayed, M. A. *J. Phys. Chem. C* **2007**, *111*, 8934–8941.
- (8) Hashimoto, S.; Uwada, T.; Hagiri, M.; Takai, H.; Ueki, T. *J. Phys. Chem. C* **2009**, *113*, 20640–20647.
- (9) Hashimoto, S.; Uwada, T.; Hagiri, M.; Shiraishi, R. *J. Phys. Chem. C* **2011**, *115*, 4986–4993.
- (10) Ko, S. H.; Choi, Y.; Hwang, D. J.; Grigoropoulos, C. P. *Appl. Phys. Lett.* **2006**, *89*, 141126.
- (11) Yamada, K.; Itoh, T.; Tsuboi, Y. *Appl. Phys. Express* **2008**, *1*, 087001.
- (12) Kotaidis, V.; Dahmen, C.; Von Plessen, G.; Springer, F.; Plech, A. *J. Chem. Phys.* **2006**, *124*, 184702.
- (13) Lukaianova-Hleb, E.; Hu, Y.; Latterini, L.; Tarpani, L.; Lee, S.; Drezek, R. A.; Hafner, J. H.; Lapotko, D. O. *ACS Nano* **2010**, *4*, 2109–2123.
- (14) Chang, S.-S.; Chen, C.-D.; Lai, W.-C.; Wang, C. R. C. *Langmuir* **1999**, *15*, 701–709.
- (15) Link, S.; Burda, C.; Mohamed, M. B.; Nikoobakht, B.; El-Sayed, M. A. *J. Phys. Chem. A* **1999**, *103*, 1167–1170.
- (16) Amendola, V.; Meneghetti, M. *Phys. Chem. Chem. Phys.* **2009**, *11*, 3805–3821.

- (17) Semaltianos, N. G. *Crit. Rev. Solid State Mater. Sci.* **2010**, *35*, 105–124.
- (18) Sasaki, K.; Takada, N. *Pure Appl. Chem.* **2010**, *82*, 1317–1327.
- (19) Asahi, T.; Sugiyama, T.; Masuhara, H. *Acc. Chem. Res.* **2008**, *41*, 1790–1798.
- (20) Takami, A.; Kurita, H.; Koda, S. *J. Phys. Chem. B* **1999**, *103*, 1226–1232.
- (21) Inasawa, S.; Sugiyama, M.; Yamaguchi, Y. *J. Phys. Chem. B* **2005**, *109*, 9404–9410.
- (22) Inasawa, S.; Sugiyama, M.; Noda, S.; Yamaguchi, Y. *J. Phys. Chem. B* **2006**, *110*, 3114–3119.
- (23) Pyatenko, A.; Yamaguchi, M.; Suzuki, M. *J. Phys. Chem. C* **2009**, *113*, 9078–9085.
- (24) Werner, D.; Hashimoto, S.; Uwada, T. *Langmuir* **2010**, *26*, 9956–9963.
- (25) Kamat, P. V.; Fluminani, M.; Hartland, G. V. *J. Phys. Chem. B* **1998**, *102*, 3123–3128.
- (26) Yamada, K.; Tokumoto, Y.; Nagata, T.; Mafune, F. *J. Phys. Chem. B* **2006**, *110*, 11751–11756.
- (27) Yamada, K.; Miyajima, K.; Mafune, F. *J. Phys. Chem. C* **2007**, *111*, 11246–11251.
- (28) Shoji, M.; Miyajima, K.; Mafune, F. *J. Phys. Chem. C* **2008**, *112*, 1929–1932.
- (29) Muto, H.; Miyajima, K.; Mafune, F. *J. Phys. Chem. C* **2008**, *112*, 5810–5815.
- (30) Giannanco, F.; Giorgetti, E.; Marsili, P.; Giusti, A. *J. Phys. Chem. C* **2010**, *114*, 3354–3363.
- (31) Werner, D.; Hashimoto, S. *J. Phys. Chem. C* **2011**, *115*, 5063–5072.
- (32) Werner, D.; Furube, A.; Okamoto, T.; Hashimoto, S. *J. Phys. Chem. C* **2011**, *115*, 8503–8512.
- (33) Matsuo, N.; Muto, H.; Miyajima, K.; Mafune, F. *Phys. Chem. Chem. Phys.* **2007**, *9*, 6027–6031.
- (34) Sasaki, K.; Nakano, T.; Soliman, W.; Takada, N. *Appl. Phys. Express* **2009**, *2*, 046501.
- (35) Soliman, W.; Takada, N.; Sasaki, K. *Appl. Phys. Express* **2010**, *3*, 035201.
- (36) Goto, M.; Ishida, S.; Tamai, N.; Matsuki, H.; Kaneshina, S. *Langmuir* **2011**, *27*, 1592–1598.
- (37) Bohren, C. F.; Huffman, D. R. *Absorption and Scattering of Light by Small Particles*; Wiley: New York, 1983.
- (38) Weingartner, H.; Franck, E. U. *Angew. Chem., Int. Ed.* **2005**, *44*, 2672–2692.
- (39) Ghosh, S. K.; Pal, T. *Chem. Rev.* **2007**, *107*, 4797–4862.
- (40) Atkins, P. W. *Physical Chemistry*, 4th ed., Oxford University Press: Oxford, 1990.
- (41) Boboridis, K.; Pottlacher, G.; Jaeger, H. *Int. J. Thermophys.* **1999**, *20*, 1289–1297.
- (42) In addition to T_{bp} , the specific heat capacity at constant pressure, thermal conductivity, and the density of water increase as the pressure increases (see, for instance: Haar, L.; Gallagher, J. S.; Kell, G. S. *NBS/NRC Steam Tables*; Hemisphere Publishing: Tacoma, WA, 1976). As a result, heat losses from Au NPs to the surrounding water increase. This may also contribute to the difficulty in particle heating at high pressures.
- (43) Schlosser, H.; Vinet, P.; Ferrante, J. *Phys. Rev. B* **1989**, *40*, 5929–5935.
- (44) Japel, S.; Schwager, B.; Boehler, R.; Ross, M. *Phys. Rev. Lett.* **2005**, *95*, 167801.
- (45) Errandonea, D. *J. Appl. Phys.* **2010**, *108*, 033517.
- (46) Caupin, F.; Herbert, E. C. *R. Phys.* **2006**, *7*, 1000–1017.
- (47) Siems, A.; Weber, S. S. L.; Boneberg, J.; Plech, A. *New J. Phys.* **2011**, *13*, 043018.
- (48) Neumann, J.; Brinkmann, R. *J. Appl. Phys.* **2007**, *101*, 114701.
- (49) Lapotko, D. *Opt. Express* **2009**, *17*, 2538–2556.
- (50) Kotaidis, V.; Plech, A. *Appl. Phys. Lett.* **2005**, *87*, 313102.
- (51) Plech, A.; Kotaidis, V.; Grésillon, S.; Damen, C.; Plessen, G. *Phys. Rev. B* **2004**, *70*, 195423.
- (52) Ekici, O.; Harrison, R. K.; Durr, N. J.; Eversole, D. S.; Lee, M.; Ben-Yakar, A. *J. Phys. D: Appl. Phys.* **2008**, *41*, 185501.
- (53) Juvé, V.; Scardamaglia, M.; Maioli, P.; Crut, A.; Merabia, S.; Joly, L.; Del Fatti, N.; Vallée, F. *Phys. Rev. B* **2009**, *80*, 195406.
- (54) Hu, M.; Hartland, G. V. *J. Phys. Chem. B* **2002**, *106*, 7029–7033.